Available online at www.sciencedirect.com
ScienceDirect
Journal of Nuclear Materials 374 (2008) 101–108
journal of nuclear materials
www.elsevier.com/locate/jnucmat

Study of a phosphate-based material with rhabdophane structure for caesium immobilization: Synthesis, sintering and leaching behaviour

Lionel Campayo [a,*], Fabienne Audubert [b], Jean-Eric Lartigue [c], Stéphanie Botuha [a], Didier Bernache-Assollant [d]

[a] CEA Marcoule, DEN/DTCD/SECM/LM2C, 30 207 Bagnols sur Ceze, France
[b] CEA Cadarache, DEN/DEC/SPUA/LTEC, 13 108 Saint Paul Lez Durance, France
[c] CEA Marcoule, DEN/DTCD/SECM/LCLT, 30 207 Bagnols sur Ceze, France
[d] ENSM-SE, Centre CIS, 158 cours Fauriel, 42 023 Saint-Etienne cedex 2, France

Received 22 May 2007; accepted 18 July 2007

Abstract

A phosphate-based material with rhabdophane structure, $K_{(1-x)}Cs_xCaNd(PO_4)_2$, was investigated as a possible host matrix for caesium extracted from reprocessed spent fuel. Its synthesis was studied by means of thermogravimetry, X-ray diffraction and scanning electronic microscopy for 'x' values comprised between 0 and 0.33. These characterizations show that both potassium and caesium are incorporated with the expected ratio and that the thermal stability extends to 1373 K. Two transient phases are identified: a monazite-type compound, $NdPO_4$ and a soluble phosphate, $K_{(1-x)}Cs_xCaPO_4$. Several heatings at 1173 K for 6 h lead to the incorporation of only 80% of caesium in the rhabdophane compound. The rhabdophane-like phase has a leach rate which ranges from 1.15 g m^{-2} d^{-1} to 8.2×10^{-3} g m^{-2} d^{-1} at 373 K depending on the surface taken into account which could be satisfactory. However, the yield of the reaction is still too low and needs to be improved to avoid the formation of soluble phosphates of which the presence is redhibitory. Dry methods do not seem to be compatible with this objective and other routes should be studied.

PACS: 81.05.Je; 81.40.−z; 81.20.Ev

1. Introduction

With a radioactive period of 2.3 million years [1], ^{135}Cs is among the fission products with the longest half-life. In France, one of the strategies investigated for the management of such radionuclides consists in an enhanced partitioning from high-level liquid waste followed by an immobilization in a specific host matrix for storage in a deep geological repository [2]. Consequently, a host matrix with a high chemical durability is required to prevent caesium release toward the biosphere. A previous work had already studied apatite-structured compounds with this objective [3]. This study highlighted the formation of a caesium–calcium–neodymium substituted double phosphate $CsCaNd(PO_4)_2$. This phosphate has a rhabdophane-like structure [4] with large channels running along the 'c' axis of the hexagonal cell which enables caesium incorporation [5]. As this phase remained in the apatitic material at the end of a leach test performed at 373 K in a soxhlet extractor [3], further characterizations strengthened the idea of its potential use as a caesium host matrix [6].

As several alkaline cations could be extracted simultaneously to caesium, the versatility of the rhabdophane-like compounds towards the incorporation of these elements needed to be evaluated. Another benefit of the partial substitution of caesium by other alkaline cations could be the decrease of the global heat output due to the decay of ^{137}Cs which is present with ^{135}Cs and could lead to unacceptable

* Corresponding author. Tel.: +33 (0)4 66 79 69 07; fax: +33 (0)4 66 79 18 80.
E-mail address: lionel.campayo@cea.fr (L. Campayo).

0022-3115/$ - see front matter © 2007 Elsevier B.V. All rights reserved.
doi:10.1016/j.jnucmat.2007.07.019

temperatures during the first decades of repository. The substitution of caesium for potassium in a solid solution with a composition of formula $K_{(1-x)}Cs_xCaNd(PO_4)_2$ ($0 \leqslant x \leqslant 0.33$) was here considered. In order to understand the behaviour of the material during its sintering or the leach test, the determination of caesium distribution at the end of the synthesis step was carefully examined.

2. Experimental

2.1. Starting materials for the synthesis $K_{(1-x)}Cs_xCaNd(PO_4)_2$ ($0 \leqslant x \leqslant 0.33$)

The different samples were synthesized from stoichiometric amounts of the following reactants: KNO_3 (99%, Merck, Germany), $CsNO_3$ (99%, Merck, Germany), $CaCO_3$ (99%, Rectapur, Prolabo, France), Nd_2O_3 (99%, Merck, Germany), Al_2O_3 (99%, Merck, Germany) and $(NH_4)_2$ HPO_4 (99%, Normapur, Prolabo, France). However, it should be noted that neodymium oxide was dehydrated at 1273 K for 3 h before weighing because of the presence of neodymium hydroxide as a secondary phase. The synthesis reaction can be written as

$$(1-x)KNO_3 + xCsNO_3 + CaCO_3 + \frac{1}{2}Nd_2O_3 + 2(NH_4)_2HPO_4 \rightarrow K_{(1-x)}Cs_xCaNd(PO_4)_2 + \frac{1}{2}N_2O_5 + CO_2 + 4NH_3 + 3H_2O \quad (1)$$

with $0 \leqslant x \leqslant 0.33$.

After weighing, reactants were mixed in porcelain mortars with acetone and dried at 373 K for one night. The samples were then heated to 1173 K for 6 h in platinum crucibles.

2.2. Characterizations

The synthesis reaction was followed by thermogravimetric analysis (TGA) to pinpoint the thermal stability of the materials and determine the temperature of the heat treatment. The samples were subsequently characterized using X-ray diffraction (XRD) to determine the phase composition and the cell parameters and then, further analyzed by scanning electronic microscopy (SEM) associated with an energy dispersive X-ray (EDX) analyzer for the microanalysis.

TGA was performed on a Setaram TG-DTA 92-16.18 analyzer. A few milligrams of the dried mixture of reactants (50×10^{-3} g) were introduced into a platinum crucible and then heated in air at a rate of 10 K/min. The crystalline phases in the heat-treated powders were identified using a Brüker AXS D8 Advance diffractometer ($\lambda_{Cu} = 1.5406$ Å). Cell parameters were determined from Brüker AXS software Eva 6.0 using SrF_2 as an internal standard. Before being observed by SEM, samples were carbon-coated. Images were acquired on a Philips XL30 equipped with an Oxford Instruments EDX Isis analyzer. The sinterability was assessed by means of the shrinkage curve of a pellet of 10^{-2} m in diameter, pressed under 100 MPa, using a Setaram TMA 92-16.18 analyzer.

Leaching experiments were performed at 373 K on sintered pellets using a stainless steel soxhlet extractor apparatus where leaching solution was distilled water. Duration of the test varied from 35 days to 37 days. An overview about this procedure is more precisely described in [7]. These experiments were done in two steps: the first seven days allowed to determine the behaviour of potentially highly soluble secondary compounds; after this period, the boiler was changed without stopping the experiment. Finally, the dissolution rate of the most durable caesium host phase was measured during the remaining time of the test.

The normalized weight loss, here given in the case of caesium, was calculated as

$$NL_{Cs} = \frac{m_{Cs}}{f_{Cs}A},$$

where NL_{Cs} is the normalized weight loss based on caesium release (g m^{-2}); m_{Cs} is the weight of caesium in the leachate (g); f_{Cs} is the mass concentration of caesium in the waste form; and A is the surface area of the sample (m^2). The dissolution rate (viz. the leach rate) R_{Cs} (g m^{-2} d^{-1}) is then given by the slope of the normalized weight loss as a function of time t (d)

$$R_{Cs} = \frac{dNL_{Cs}}{dt}.$$

Caesium was chosen as an indicator of the dissolution of the soluble fraction during the first part of the test as well as the more durable phase during the second period because it is not incorporated in precipitated by-products. Only the dissolution rate (R_{Cs}) of the most durable phase, determined from the second part of the leaching test procedure, after the change of the boiler, will be considered. This value is calculated from the linear part of the normalized weight loss curve by a least squares-based algorithm ($R^2 > 0.65$).

Caesium and calcium were measured out by atomic absorption spectroscopy and phosphorus by inductively coupled plasma mass spectrometry. Neodymium data is not presented because the concentrations were under the detection limits. Potassium was not measured out.

Measurement of specific area for powders was performed on a MicromeritiCs GEMINI 2360 using nitrogen adsorption. Surface area for sintered bodies was measured by krypton adsorption at the Pôle de Ressources Industriel Matériaux et VERRE (Montpellier, France). Apparent powder density was determined by He-pycnometry on a MicromeritiCs ACCUPYC 1330.

3. Results and discussion

3.1. Study of the solid solution $K_{(1-x)}Cs_xCaNd(PO_4)_2$ ($0 \leqslant x \leqslant 0.33$)

Fig. 1 shows a typical TGA curve of the synthesis of the solid solution $K_{(1-x)}Cs_xCaNd(PO_4)_2$ ($0 \leqslant x \leqslant 0.33$) for the

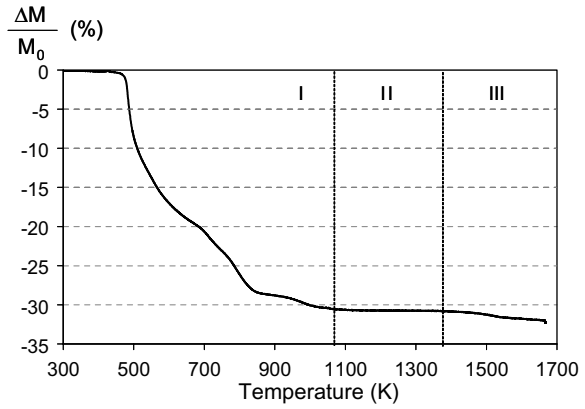

Fig. 1. TGA of the $K_{0.92}Cs_{0.08}CaNd(PO_4)_2$ composition. I : $\frac{(M-M_0)}{M_0} < \Delta M_{th}$; II(plateau) : $\frac{(M-M_0)}{M_0} = \Delta M_{th}$; III : $\frac{(M-M_0)}{M_0} > \Delta M_{th} \Delta M_{th}$: theoretical mass loss.

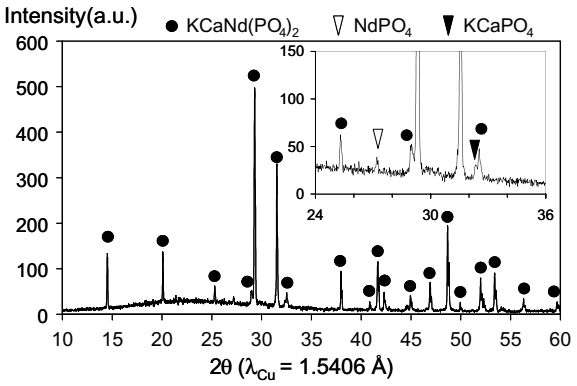

Fig. 2. XRD pattern of '$K_{0.92}Cs_{0.08}CaNd(PO_4)_2$' reactant mixture Eq. (1) after annealing at 1173 K for 6 h.

particular composition $K_{0.92}Cs_{0.08}CaNd(PO_4)_2$. After the decomposition of the nitrates and carbonates, corresponding to the first temperature range (I), a plateau for which expected and measured mass losses are equal (II), is observed. The calculation of the expected mass loss is based on the theoretical synthesis reaction and takes into account $(NH_4)_2HPO_4$ partial dissociation during the drying step at 373 K according to the following reaction:

$$(NH_4)_2HPO_4 \rightarrow NH_4H_2PO_4 + NH_3.$$

At the end of the plateau a new mass loss is identified on the TGA curve and this event was assigned to the decomposition of the freshly synthesized phases (III). Whatever the composition which was considered, TGA data point out that no significant difference was found between expected and observed mass loss (viz. greater than 0.2%) between room temperature and 1073 K (Table 1).

This indicates that, for short heating times, volatilization phenomena could be assumed as negligible. The thermal stability for all the studied compositions was higher than 1373 K which is satisfactory enough regarding the radioactive caesium heat output.

Considering this result, the dried mixtures of the reactants were annealed at 1273 K for 18 h and characterized by XRD. Fig. 2 shows the XRD pattern for the sample corresponding to $KCaNd(PO_4)_2$. From the comparison with the ICDD card 34-0112, the main phase detected was effectively assigned to the rhabdophane-like double phosphate $KCaNd(PO_4)_2$. However, two other compounds were also identified: a monazite-type phosphate with $NdPO_4$ formula and another phosphate corresponding to $KCaPO_4$. These two latter phases should be considered as transient compounds to form the rhabdophane-structured phase. Such a mechanism was already established in a former work for the entirely caesium-substituted compound $CsCaNd(PO_4)_2$ [6]. The reaction can then be rewritten as

$$NdPO_4 + KCaPO_4 \rightarrow KCaNd(PO_4)_2.$$

Similar trends were observed for the other studied compositions ($0 \leqslant x \leqslant 0.33$) and that is why it was assumed that the same mechanism was also involved.

Table 2 shows the cell parameters obtained for the hexagonal system as a function of the composition. A linear increase of the '*a*' parameter and a linear decrease of the '*c*' parameter are observed for increasing values of '*x*' (Fig. 3). This trend is in agreement with an increase of the mean ionic radius of the alkaline cation when the caesium amount increases in the material. This phenomenon was also described by Keller et al. [5] for related rhabdophane compositions. These authors suggested that the structure could expand and contract more easily along the [1 0 0] direction. This statement is confirmed by our results which show a stronger effect of the increase of the mean ionic radius on the '*a*' parameter than on the '*c*'

Table 1
TGA data of the solid solution $K_{(1-x)}Cs_xCaNd(PO_4)_2$ ($0 \leqslant x \leqslant 0.33$) synthesis

x	$\Delta M_{th.}$ (%)[a]	ΔM_{exp} (%)[b]	T_{min} (K)[c]	T_{max} (K)[d]
0	31.04	30.90	1043	>1773
0.08	30.65	30.69	1083	1406
0.16	30.27	30.21	1080	1423
0.25	29.87	29.82	1056	1459
0.33	29.51	29.53	1063	1443

[a] Theoretical weight loss ($(NH_4)_2HPO_4$ decomposition into $NH_4H_2PO_4$ before the analysis was performed was taken into account).
[b] Observed weight loss between room temperature and 1073 K.
[c] Temperature of the beginning of the plateau on the thermogravimetric curve after decomposition of the reactants.
[d] Thermal stability limit.

Table 2
Cell parameters (hexagonal system) of the rhabdophane-like phase as a function of the composition

x	a (Å) (±0.002)	c (Å) (±0.002)
0	7.020	6.409
0.08	7.030	6.404
0.16	7.038	6.401
0.25	7.045	6.398
0.33	7.050	6.392

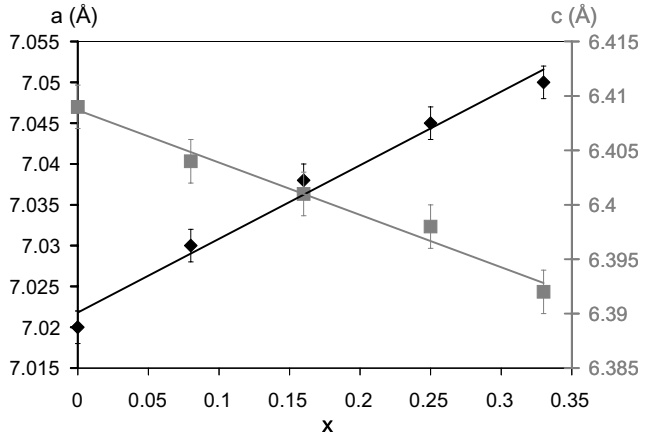

Fig. 3. Evolution of the cell parameters (hexagonal system) along the $K_{(1-x)}Cs_xCaNd(PO_4)_2$ solid solution for 'x' values between 0 and 0.33.

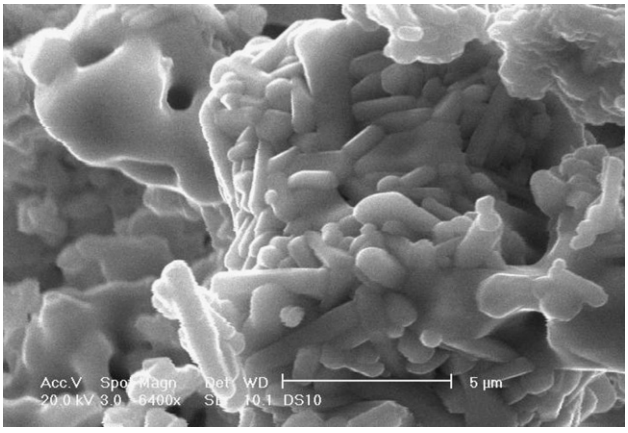

Fig. 4. SEM micrograph of the $K_{0.67}Cs_{0.33}CaNd(PO_4)_2$ composition issued from the synthesis route described by Eq. (1) annealed at 1273 K for 18 h.

parameter. Finally, these observations were found to be consistent with an effective increase of the caesium amount within the rhabdophane structure along the solid solution, from $KCaNd(PO_4)_2$ to $K_{0.67}Cs_{0.33}CaNd(PO_4)_2$. In order to determine the K/Cs ratio in the rhabdophane-like phase, the heat-treated samples were observed by SEM and analyzed by EDX.

Fig. 4 shows a typical observation of these samples for the solid solution $K_{(1-x)}Cs_xCaNd(PO_4)_2$ ($0 \leqslant x \leqslant 0.33$) in the particular case of the $K_{0.67}Cs_{0.33}CaNd(PO_4)_2$ composition. The rhabdophane grains are unambiguously identified on this micrograph thanks to their characteristic rod-shaped crystals. Their microanalysis is presented in Table 3. This characterization confirms that the K/Cs ratio is close to the expected value and that caesium and potassium are simultaneously incorporated in the rhabdophane. Neodymium amount seems to be higher than the theoretical value and this could be explained by the presence of free neodymium oxide/hydroxide in the near surface of the analyzed grains. The microanalysis also reveals the presence of secondary phases. In agreement with XRD analysis, a phosphate with a composition close to $KCaPO_4$ was found in all samples. This phase contains small amounts of caesium increasing with 'x'. If the synthesis mechanism of the rhabdophane phase involves the preliminary formation of monazite and $K_{(1-x)}CsxCaPO_4$ the caesium amount immobilized in $K_{(1-x)}Cs_xCaPO_4$-type compounds is lower than that could be expected. This can be explained by the partial volatilization of this element in the near surface due to a long heating time of 18 h at 1273 K. The loss of alkaline cations in $M^IM^{II}PO_4$ (M^I = K, Rb, Cs; M^{II} = Ca, Eu)-type phases with temperature was already reported by some authors [6,8]. The release of the alkaline cation M^I leads to the formation of a whitlockite-type phase, $M^{II}{}_3(PO_4)_2$. In the present work, in the case of $K_{(1-x)}Cs_xCaPO_4$ it is shown that caesium is released first because of a higher volatility of this element compared to potassium. The $K_{(1-x)}Cs_xCaPO_4/Ca_3(PO_4)_2$ conversion kinetics seems to increase with the increase of 'x'. De facto, for $x = 0.25$, a $Ca_{10}K(PO_4)_7$-type phase which is isostruc-

Table 3
Structural formula of the different phases which were identified from their EDX microanalysis spectrum

x	Phase	K	Cs	Ca	Nd	P	O	Assignment
0	1	0.98 (0.05)	–	0.96 (0.01)	0.07 (0.02)	0.98 (0.01)	4	$KCaPO_4$
	2	0.91 (0.04)	–	0.96 (0.04)	1.30 (0.08)	1.85 (0.05)	8	Rhabdophane
0.08	1	1.01 (0.04)	0.01 (0.01)	1.00 (0.03)	0.03 (0.01)	0.97 (0.01)	4	$KCaPO_4$
	2	0.82 (0.08)	0.09 (0.01)	0.98 (0.14)	1.27 (0.12)	1.86 (0.04)	8	Rhabdophane
0.16	1	1.03 (0.05)	0.04 (0.01)	1.02 (0.04)	0.06 (0.02)	0.95 (0.02)	4	$KCaPO_4$
	2	0.78 (0.06)	0.18 (0.01)	0.98 (0.07)	1.34 (0.08)	1.82 (0.04)	8	Rhabdophane
0.25	1[a]	0.91	0.06	1.05	0.04	0.97	4	$KCaPO_4$
	2	0.70 (0.07)	0.24 (0.03)	0.96 (0.04)	1.30 (0.06)	1.85 (0.05)	8	Rhabdophane
	3	1.00 (0.04)	0.12 (0.04)	10.00 (0.13)	0.27 (0.08)	6.80 (0.08)	28	$Ca_{10}K(PO_4)_7$
0.33	1[a]	1.00	0.10	0.99	0.05	0.96	4	$KCaPO_4$
	2	0.68 (0.02)	0.34 (0.02)	0.99 (0.02)	1.29 (0.03)	1.83 (0.03)	8	Rhabdophane
	3[b]	2.20	0.50	23.29	0.75	13.57	59.69	?

Values in parenthesis give standard deviation for seven to ten analyzed grains.
[a] Standard deviation is not given for these phases since only a grain was analyzed.
[b] This phase was not assigned to a defined compound. Only the atomic weight percent is listed.

tural to whitlockite, $Ca_3(PO_4)_2$ was detected. Such a compound was not observed for lower values of 'x'. The following equations, written for $x = 0.25$, can be proposed to describe the overall process:

$$30K_{0.75}Cs_{0.25}CaPO_4 \rightarrow 3Ca_{10}K_{0.75}Cs_{0.25}(PO_4)_7 + 9(0.75K_3PO_4, 0.25Cs_3PO_4)(\uparrow),$$

$$3Ca_{10}K_{0.75}Cs_{0.25}(PO_4)_7 \rightarrow 10Ca_3(PO_4)_2 + (0.75K_3PO_4, 0.25Cs_3PO_4)(\uparrow).$$

It should be noted that these equations do not take into account caesium volatilization which leads to an enrichment in potassium in the solid.

3.2. Study of '$K_{0.67}Cs_{0.33}CaNd(PO_4)_2$'

The choice of $K_{0.67}Cs_{0.33}CaNd(PO_4)_2$ as a standard composition was done because it corresponds to a caesium load of 10 wt% and it is not suitable to increase this value. De facto, the global heat output of a radioactive waste in which isotopic spectrum includes high amounts of ^{137}Cs limits the caesium amount that can be incorporated in a host matrix. As described in the previous paragraph, the rhabodphane-like phase $K_{0.67}Cs_{0.33}CaNd(PO_4)_2$ can be obtained according to the following equation:

$$0.67KNO_3 + 0.33CsNO_3 + CaCO_3 + \frac{1}{2}Nd_2O_3 + 2(NH_4)_2HPO_4 \rightarrow K_{0.67}Cs_{0.33}CaNd(PO_4)_2 + \frac{1}{2}N_2O_5 + CO_2 + 4NH_3 + 3H_2O.$$

This synthesis route will be called 'R-mode'. Nevertheless, the formation of this compound involves two transient phases which are the Nd-monazite and $K_{0.67}Cs_{0.33}CaPO_4$. That is why another synthesis route might consist in the following reaction:

$$K_{0.67}Cs_{0.33}CaPO_4 + NdPO_4 \rightarrow K_{0.67}Cs_{0.33}CaNd(PO_4)_2.$$

It will be called 'D-mode'. To study this specific route, each transient phase was specifically prepared. Nd-monazite was obtained from a solid state reaction at 1673 °C for 6 h between Nd_2O_3 and $(NH_4)_2HPO_4$ with an Nd/P molar ratio equal to 1. For $K_{0.67}Cs_{0.33}CaPO_4$ a two-step synthesis was developed with the same protocol used by Jinlong et al. [9] for $K_{0.5}Na_{0.5}CaPO_4$. In this way, 0.5 $CaHPO_4 \cdot 2H_2O$, 0.335 K_2CO_3 0.165 Cs_2CO_3 and 0.5 $CaCO_3$ were first mixed in distilled water at room temperature. Then, stoichiometric amounts of H_3PO_4 (85%) were slowly added and the solution was allowed to cure for half an hour before being dried at 393 K for one night. Finally, this intermediate was heated at 1223 K for 6 h. As alkaline carbonates which have been used for this synthesis are highly hygroscopic, they were beforehand dehydrated at 573 K before weighing.

3.2.1. Chemical efficiency

In order to quantify the chemical efficiency of the reaction, that is to say the effective amount of rhabdophane finally synthesized compared to secondary by-products ($NdPO_4$ $K_{0.66}Cs_{0.33}CaPO_4$), a specific protocol was developed.

Whatever the synthesis route, either R-mode, either D-mode, the starting mixture was heated at 1173 K during 2 h. The samples were heated several times with intermediate grinding and pelletizing to improve the reaction. The grinding was performed in ethanol with a S-1/2 type or MM-2 type Retsch™ grinder. One gram of raw material was sampled between some heatings to undergo a washing. One gram of powder was washed with 20 mL of distilled water under magnetic stirring for half an hour at room temperature ($S/V < 50\ cm^{-1}$). Liquid phase was then collected and analyzed by inductively coupled plasma atomic absorption spectroscopy. This was done to determine the instantaneously released caesium fraction (IRCsF) as a function of the number of heatings.

On one hand, monazites are quite insoluble in geological environments [10] and the behaviour of $CsCaNd(PO_4)_2$ in leaching conditions was considered to be satisfactory in a previous work [3]. On another hand, Wu et al. [8] have already shown that M^IEuPO_4 (M^I = K, Rb, Cs), isotype of $K_{0.66}Cs_{0.33}CaPO_4$ could be easily dissolved. The mechanism of the hydrolysis of $K_{(1-x)}Cs_xCaPO_4$ can be described by the following general equations (here given for $CsCaPO_4$):

$$5CsCaPO_4 \rightarrow 5Cs^+ + 5Ca^{2+} + 5PO_4^{3-},$$

$$5Ca^{2+} + 3PO_4^{3-} + OH^- \rightarrow Ca_5(PO_4)_3(OH)(\downarrow).$$

That is why a high IRCsF can be associated to the presence of $K_{0.66}Cs_{0.33}CaPO_4$ and yet is a good indicator of the degree of conversion for the reaction which proceeds by progressive consumption of $K_{0.66}Cs_{0.33}CaPO_4$.

Fig. 5 shows the evolution of the IRCsF by normalization to the caesium initial amount in the case of a R-mode prepared powder. It is compared to the evolution of an entirely substituted Cs-rhabodphane, $CsCaNd(PO_4)_2$. Trends are similar for the two studied compositions and show high IRCsF values; the reaction is incomplete even

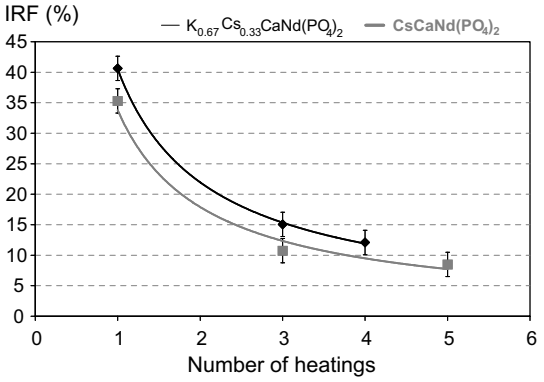

Fig. 5. Instantaneously released caesium fraction (IRF) as a function of the number of heatings for $K_{0.67}Cs_{0.33}CaNd(PO_4)_2$ and $CsCaNd(PO_4)_2$ for a R-mode synthesis.

in the case of five consecutive heatings. Nonetheless, one can note that a significant decrease of the IRCsF is observed for the three first heatings but then, this protocol seems to be less and less efficient.

It is important to note that the IRCsF presented here is probably underestimated because the washing might not be optimized. Consequently, only a trend can be deduced. However, this characterization shows that a direct evaluation of rhabdophane leach resistance from the release of caesium should take into account the remaining presence of $K_{0.67}Cs_{0.33}CaPO_4$ and consequently, might be impossible. That is why a specific protocol with two steps was used (see Section 2.2) for this experiment. For the first seven days of the test, the release of caesium is mainly due to the dissolution of $K_{0.67}Cs_{0.33}CaPO_4$. The own behaviour of the rhabdophane-like phase can only be determined after the change of boiler at the end of this time, which allows the system to 'forget' the initial leaching.

3.2.2. Sinterability of the $K_{0.67}Cs_{0.33}CaNd(PO_4)_2$ composition

Rhabdophane samples with $K_{0.67}Cs_{0.33}CaNd(PO_4)_2$ composition were prepared according to the R-mode or D-mode in order to compare the synthesis route influence on sintering. Aluminum comes from the grinding which is responsible for a slight contamination of the samples with alumina.

Table 4 summarizes some physical characterizations of the powders at the end of the series of heatings. Surface areas are quite similar whatever the synthesis route and vary from 1.3 m^2/g to 1.6 m^2/g whereas apparent density is close to the theoretical value of 4.01 which can be calculated using a linear regression with $\rho_{th} = 3.764$ for $KCaNd(PO_4)_2$ and $\rho_{th} = 4.504$ for $CsCaNd(PO_4)_2$. Slightly higher values for D-mode prepared powders can be interpreted in terms of a higher contamination with alumina (see Table 5). Fig. 6 shows the typical shrinkage of a pellet uniaxially pressed under 10×10^6 Pa in the case of a R-mode synthesis route. Shrinkage due to sintering begins at 1070 K and is not finished at the maximum temperature of 1465 K. Such a temperature is higher than the thermal stability determined by TGA (see Table 1). This means that the sintering temperature range partially overlaps the decomposition of the material above 1440 K. The derived curve of the shrinkage also enables to identify an increase of the densification rate within the temperature range 1333–1398 K. Such behaviour can be assigned to the melting of $K_{0.67}Cs_{0.33}CaPO_4$ which remains in the material followed by its transformation into a whitlockite-type compound. A clear evidence of this assumption is that this increase disappears if the powder was first washed before performing TMA. The return to a normal the densification rate above 1398 K can be linked to the end of this conversion. Similar trends are observed for all the studied samples.

Relative densities are close for R and D samples (88.5% and 85.9%, respectively). In none case, the relative density was found higher than 92% which implies the presence of an opened porosity in the sintered bodies. A too large proportion of $K_{0.67}Cs_{0.33}CaPO_4$-type phase into the material was assumed to be responsible for the low value obtained. This porosity can then contribute to the reactive surface during the leach test. Moreover, an increase in porosity is expected with the dissolution of $K_{0.67}Cs_{0.33}CaPO_4$.

Table 4
Powders characteristics for sinterability studies

Synthesis way	R-mode	D-mode
Sample	R	D
Annealing	(1173 K-2 h) × 5	(1173 K-2 h) × 2 + (1173 K-6 h) × 4
S_{BET} (m^2/g)	1.3	1.6
ρ (g/cm^3)	4.01	4.10

Table 5
Sintered bodies characteristics

Sample	R	D
Sintering conditions[a]	1423 K-12 h	1403 K-7 h
Relative density (%)[b]	88.5	85.9
Chemical analysis (wt%)[c]	K: 6.06; Cs: 7.56; Ca:8.53; Nd: 29.90; P: 14.00; Al: 3.38	K: 5.70; Cs: 7.26; Ca:8.22; Nd: 29.30; P: 13.19; Al: 3.95

[a] Powders were initially pressed under 100 MPa into pellets of 2×10^{-2} m in diameter before heating.

[b] Relative density is the ratio between the apparent density of the sintered pellet and the density of the powder determined by He-pycnometry; the apparent density of the sintered pellet is determined from dimensional measurements.

[c] The different elements were measured out by inductively coupled plasma optical emission spectroscopy at the Centre Européen de Recherche et d'Enseignement de Géosciences de l'Environnement (Aix-en-Provence, France).

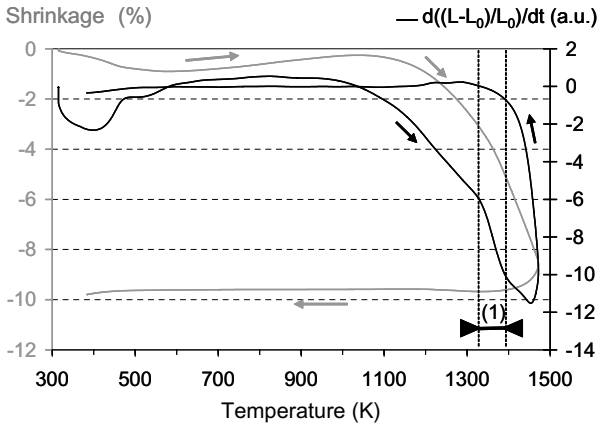

Fig. 6. Densification behaviour of the $K_{0.67}Cs_{0.33}CaNd(PO_4)_2$ composition issued from the synthesis route described by Eq. (1) (annealing: five cycles (1173 K-2 h); initially pressed to a pellet of 10^{-2} m in diameter under 100 MPa). (1): Melting of $K_{(1-x)}Cs_xCaPO_4$-type phase.

3.2.3. Leaching properties of the $K_{0.67}Cs_{0.33}CaNd(PO_4)_2$ composition

The amount of released caesium after the first sequence of seven days was determined after acidification and by analyzing the solution in the boiler. It reaches 22.0% and 18.5% of the initial amount in the solid for R and D samples, respectively. These values count for the IRCsF due to the quick hydrolysis of $K_{0.66}Cs_{0.33}CaPO_4$. One can note that they are very close and no significant influence of the synthesis mode was underlined. This could be explained by the accumulation of grindings and heatings which erased the initial differences between each synthesis mode.

During the second sequence the own behaviour of $K_{0.67}Cs_{0.33}CaNd(PO_4)_2$ was characterized. Figs. 7 and 8 show the normalized weight losses for caesium release and for calcium and phosphorus release as a function of the leaching time respectively. These values take into account the first sequence of seven days before the change of boiler. The leach rates are equal to 1.15 and 1.36 g m^{-2} d^{-1} for D and R samples on the basis of caesium release. The leach rates deduced from phosphorus or calcium are lower, with one or two orders of magnitude less. This could be linked to the crystallographic structure of rhabdophane compounds which are composed of channels running along the '*c*' axis in which elements like caesium and potassium are more easily exchanged compared to elements of the 'skeleton' made of alkaline-earth/rare earth oxygen octahedrons and phosphate tetrahedrons. In addition, calcium and phosphorus can sometimes precipitate in the boiler during the leach test as suggested by higher amounts found after acidification compared to the sum in the sampled aliquots. The precipitation of calcium phosphates might be responsible for this statement. The reason why neodymium was not detected might also been explained by the precipitation of $NdPO_4$, $0.5H_2O$ which has the rhabdophane structure.

Taking into account the low relative density of the pellets, the assumption of the equality between the geometric surface area of the sample and the efficient surface area for water could be questionable because of the presence of opened porosity in the material. That is why the specific surface area for the D sample was measured by means of krypton adsorption before the leach test was performed. It equals 1020×10^{-4} m^2 (geometric area: 7.283×10^{-4} m^2). In fact, as the leach rates are determined for the second sequence of the experiment, it is difficult to determine the true surface because of the presence of cracks that have resulted from the dissolution of $K_{0.66}Cs_{0.33}CaPO_4$ during the first seven days before the change of boiler. Consequently, the leach rate value probably overestimates the true one. Finally, the normalized leach rate based on caesium release and for a specific surface of 1020×10^{-4} m^2 leads to a value of 8.2×10^{-3} g m^{-2} d^{-1}. The true leach rate probably lies between the assessment given by the geometric surface and that given by the specific surface which indicates good retention efficiency.

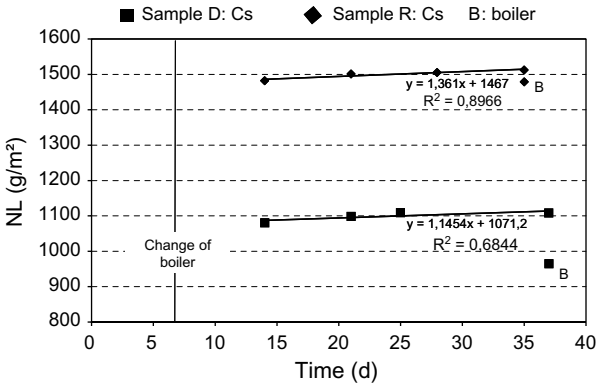

Fig. 7. Normalized weight loss based on caesium and potassium release and for the geometric surface area of the samples (7.844×10^{-4} for R sample, 7.283×10^{-4} m^2 for D sample) as a function of leaching time.

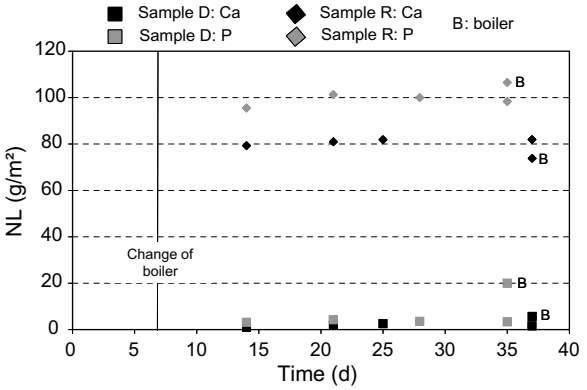

Fig. 8. Normalized weight loss based on calcium and phosphorus release and for the geometric surface area of the samples (7.844×10^{-4} for R sample, 7.283×10^{-4} m^2 for D sample) as a function of leaching time.

4. Conclusion

The existence of a solid solution of $K_{(1-x)}Cs_x$-$CaNd(PO_4)_2$ type for '*x*' values between 0 and 0.33 was demonstrated. These rhabdophane-like compounds were successfully synthesized within the temperature range 1173–1273 K with a thermal stability higher than 1373 K. A secondary Cs-bearing phase which can be written as $K_{(1-x)}Cs_xCaPO_4$ was also identified in the same time as Nd-monazite, $NdPO_4$. The rhabdophane was thus assumed to be issued from the reaction between these two transient phases. The $K_{0.67}Cs_{0.33}CaNd(PO_4)_2$ composition has been further characterized to determine its sinterability and leach resistance. The melting of $K_{0.67}Cs_{0.33}CaPO_4$ during sintering is responsible for an increase of the densification rate but a too high amount of this phase led to a relative density below the closure of opened porosity. In addition, caesium volatilization limits the sintering temperature and the relative density which can be obtained (less than 90%). As a matter of fact, after several heatings, the

reaction yield, which was assessed from the quick caesium release due to the dissolution of $K_{0.67}Cs_{0.33}CaPO_4$ during the first seven days of leaching at 373 K, is only 80%. This value represents the amount of caesium efficiently immobilized in the rhabdophane structure. Once $K_{0.67}Cs_{0.33}CaPO_4$ is removed from the system, the material shows satisfactory properties. The leach rate on the basis of caesium release is found to range from 1.15 $g\,m^{-2}\,d^{-1}$ to 8.2×10^{-3} $g\,m^{-2}\,d^{-1}$ depending on the surface taken into account. However, in order to get a suitable host matrix for caesium immobilization, the improvement of the synthesis yield and the sintering is of critical importance. Clearly, with a yield of 80%, these materials cannot be retained for this application and the incomplete conversion seems difficult to overcome by dry synthesis routes. This lack of reactivity could be explained by the segregation during the heating of monazite. Indeed, such a structure was already observed for the dry synthesis of $CsCaNd(PO_4)_2$ [6] where monazite is preferentially located in the centre of agglomerates made of rhabdophane grains in the near surface which embed the soluble phosphate. Unfortunately, the two methods here described are not successful in creating the homogeneity necessary to improve the rhabdophane formation.

Acknowledgement

The authors would like to thank Miss Hélène Juhan for its technical support during the leachates analyses.

References

[1] D.R. Lide, in: Handbook of Chemistry and Physics, 73rd Ed., CRC Press, Boca Raton (Florida (USA)), 1992, p. Section 11.
[2] Code de l'Environnement, Livre 5 (Prévention des pollutions, des risques et des nuisances), Titre IV (Déchets), Chapitre 2 (Dispositions particulières aux déchets radioactifs) (in French).
[3] L. Campayo, F. Audubert, J.E. Lartigue, D. Bernache-Assollant, J. Mater. Sci. 39 (2003) 4861.
[4] M. Vlasse, P. Bochu, C. Parent, J.P. Chaminade, A. Daoudi, G. Le Flem, P. Hagenmuller, Acta Cryst. B 38 (1982) 2328.
[5] L.P. Keller, G.J. Mc Carthy, R.G. Garvey, Mater. Res. Bull. 20 (1984) 459.
[6] L. Campayo, F. Audubert, D. Bernache-Assollant, Solid State Ionics 176 (2005) 2663.
[7] French AFNOR draft standard X 30-403.
[8] G.Q. Wu, Z. Tang, Y. Yu, P. Lin, M. Jansen, K. Königstein, Z. Anorg. Allg. Chem. 610 (1992) 135.
[9] N. Jinlong, Z. Zhenxi, J. Dazong, Y. Shenghong, W. Keguang, J. Mater. Sci. 36 (2001) 3805.
[10] E.H. Oelkers, F. Poitrasson, Chem. Geol. 191 (2002) 73.